



HAL
open science

Electrokinetic leakage as a tool to probe internal fouling in MF and UF membranes

C. Rouquie, S. Liu, Murielle Rabiller-Baudry, A. Riaublanc, M. Frappart,
Estelle Couallier, Anthony Szymczyk

► To cite this version:

C. Rouquie, S. Liu, Murielle Rabiller-Baudry, A. Riaublanc, M. Frappart, et al.. Electrokinetic leakage as a tool to probe internal fouling in MF and UF membranes. *Journal of Membrane Science*, 2020, 599, pp.117707. 10.1016/j.memsci.2019.117707 . hal-02498315

HAL Id: hal-02498315

<https://univ-rennes.hal.science/hal-02498315>

Submitted on 27 Mar 2020

HAL is a multi-disciplinary open access archive for the deposit and dissemination of scientific research documents, whether they are published or not. The documents may come from teaching and research institutions in France or abroad, or from public or private research centers.

L'archive ouverte pluridisciplinaire **HAL**, est destinée au dépôt et à la diffusion de documents scientifiques de niveau recherche, publiés ou non, émanant des établissements d'enseignement et de recherche français ou étrangers, des laboratoires publics ou privés.

Electrokinetic leakage as a tool to probe internal fouling in MF and UF membranes

C. Rouquié^{1,2,3}, S. Liu^{2,4}, M. Rabiller-Baudry¹, A. Riaublanc³, M. Frappart², E. Couallier^{2*}, A. Szymczyk^{1*}

¹Univ Rennes, CNRS, ISCR (Institut des Sciences Chimiques de Rennes) – UMR 6226, F-35000 Rennes, France

²CNRS, GEPEA, Université de Nantes, 37 Boulevard de l'université, BP 406, 44602 Saint-Nazaire cedex, France

³INRA, BIA, Rue de la Géraudière, BP 71627, 44 316 Nantes Cedex 3, France

⁴ADEME, 20 avenue du Grésillé, BP90406, 49004 Angers cedex 01, France

*Corresponding authors: anthony.szymczyk@univ-rennes1.fr, estelle.couallier@univ-nantes.fr

Abstract

Tangential electrokinetic measurements are widely used to characterize membrane fouling as the membrane zeta potential is partly governed by the presence of foulant materials on its surface. However, in the case of porous materials as micro- (MF) and ultrafiltration (UF) membranes, a part of the streaming current flows through the porosity of the membrane during measurements. This electrokinetic leakage, is directly impacted by the presence of foulant materials inside the membrane porosity. Hence, this paper investigates for the first time the possibility of using electrokinetic leakage as a probe for detecting internal fouling, taking lipid fouling as example. Firstly, a lab-scale methodology combining “upside-down” fouling experiments with electrokinetic measurements demonstrated that the intensity of the electrokinetic leakage was related to the presence of internal fouling. Secondly, the concept was applied to the pilot-scale MF and UF of an oil-in-water emulsion

23 under various transmembrane pressures (TMP). A significant impact of the TMP on the internal
24 fouling of a MF PES membrane was highlighted, whereas almost no impact of the TMP was noticed in
25 the case of an UF PAN membrane. The developed methodology using the quantification of the
26 electrokinetic leakage phenomenon allows distinguishing the contributions of internal and external
27 (surface) fouling. These findings offer new application of tangential electrokinetic measurements to
28 gain more insight into the characterization of membrane fouling.

29

30 **Highlights:**

- 31 • New characterization of internal fouling by tangential electrokinetic measurement
- 32 • Internal and external fouling contributions to membrane electrokinetic properties
- 33 • Impact of the operating transmembrane pressure on internal fouling occurrence

34

35 **Keywords:** Membrane fouling; electrokinetics; streaming current; microfiltration; ultrafiltration

36

37

38

39

40

41

42

43

44

45

46 **1 Introduction**

47 Despite the many advantages and applications of membrane filtration, performances keep being
48 hampered by membrane fouling due to deposit and/or adsorption of compounds on the membrane
49 surface and/or inside the membrane porosity. In the light of this, there is an important need of
50 characterization methods in order to strengthen membrane fouling comprehension and thus improve
51 fouling control during large-scale filtrations.

52 Many strategies have been applied so far to characterize membrane fouling, starting with
53 conventional flux/pressure monitoring often combined with prediction or comprehension models
54 (resistance-in-series, pore blocking, inertial lift models, etc.). These widely used approaches are
55 powerful tools allowing describing membrane fouling through the estimation of various parameters:
56 resistance due to membrane fouling, reversibility of membrane fouling, main fouling mechanisms,
57 filtration cake thickness and porosity, etc. However, their findings are based on estimation models
58 themselves based on macroscopic scale parameters (flux and pressure) and can be far from the
59 microscopic reality occurring around the membrane surface [1].

60 In view of the foregoing, advanced techniques allowing fouling characterization directly on the
61 membrane surface have been gaining more and more interest these past years, as they can provide
62 precise information about fouling composition, concentration and location on the membrane. The
63 major techniques used for membrane surface characterization have been reviewed by Johnson et al.
64 [2]. It includes spectroscopic techniques such as ATR-FTIR, Raman and XPS spectroscopy, mainly
65 used to investigate the chemical nature of foulant compounds, their location and even their
66 concentration on the membrane surface [3–5]. Imaging techniques (AFM, SEM, TEM, etc.) are also of
67 great interest for membrane fouling characterization as they can bring information about fouling
68 layer thickness and distribution [1]. The study of the modification of the membrane wetting
69 properties (contact angle) and electrokinetic behavior (electrophoresis, streaming and
70 sedimentation potential measurements) induced by the presence of foulant materials on its surface
71 bring useful information as well [2].

72 However, most of these techniques mainly focus on the membrane surface characterization. Few
73 studies deal with the characterization of internal fouling, even though this latter is often irreversible
74 and causes severe loss of performances and cleaning overcost. Yeo et al. [6] managed to monitor

75 external and internal organic fouling deposition on and in a hollow fiber membrane using phase-
76 contact XMI, while 3D optical coherence tomography was successfully used by Trinh et al. [7] to
77 characterize external and internal fouling during microfiltration of oil-in-water emulsions. Similarly,
78 electrochemical impedance spectroscopy has been recently used to identify the main fouling
79 mechanism (external fouling layer or irreversible internal fouling) [8]. Apart from these anecdotal
80 applications, there still is a lack of analytical strategies for internal fouling investigation. Considering
81 the well-known impact of fouling on the membrane charge, the investigation of surface and porous
82 structures zeta potentials may bring useful information for external and internal fouling
83 characterization.

84 Determining the zeta potential of a membrane provides insight into its surface electrical properties
85 in a given physicochemical environment. It is therefore of great interest when investigating problems
86 of practical relevance such as membrane fouling [9, 10] or ageing [11, 12].

87 The zeta potential of membranes can be inferred from electrokinetic techniques such as streaming
88 potential and streaming current. From the experimental point of view, the easiest way to perform the
89 electrokinetic characterization of porous membranes is to implement through-pore streaming
90 potential measurements (also known as transversal mode) [13–15]. However, the multilayer
91 structure of commercial membranes used in pressure-driven processes (micro-, ultra- and nano-
92 filtration as well as reverse osmosis) makes the determination of the skin layer properties quite tricky
93 [16–18]. In order to overcome the difficulty inherent in the analysis of through-pore measurements,
94 an alternative measuring method, known as tangential mode and based on the application of the
95 pressure gradient along the membrane skin layer (and not through the membrane thickness) has
96 been proposed and has become the most widely used technique in membrane science [19–22].

97 When considering tangential electrokinetic measurements, it has been argued that streaming current
98 should be preferred over streaming potential since this latter is likely to be impacted by the extra
99 contribution of the underlying support layer(s) to the overall electrical conductance [23, 24].
100 Tangential streaming current has been shown to be a reliable technique to highlight the presence of
101 thin coating layers onto the surface of some commercial nanofiltration and reverse osmosis
102 membranes [25]. However, complications have been pointed out when tangential streaming current
103 measurement is applied to porous materials like micro- and ultra-filtration membranes due to the
104 occurrence of a non-negligible streaming current through the membrane porosity[26–28]. This

105 parasitic contribution to the experimental signal, hereinafter referred as electrokinetic leakage, can
106 be taken into account by applying a protocol consisting in a series of measurements performed by
107 changing the distance between the two membranes samples required for tangential measurements
108 [26–28]. Such a procedure has been successfully applied by Szymczyk *et al.* (2013) to give evidence
109 for the presence of 4-benzyltriphenylphosphonium groups within pores of an ultrafiltration
110 membrane after its functionalization [28].

111 In this work, we show for the first time that the electrokinetic leakage phenomenon can be used to
112 gain insight into membrane fouling. Notably, we show that electrokinetic leakage can be used as a
113 probe to highlight the occurrence of internal fouling within the porous structure of micro- and ultra-
114 filtration membranes. The methodology followed in this work also enables distinction between
115 fouling onto the membrane surface and within the membrane pores.

116 **2 Theoretical background**

117 Tangential streaming current measurement consists in applying a pressure gradient along a channel
118 formed by two identical membrane samples facing each other and immersed in an electrolyte
119 solution. While the pressure gradient is applied along the membrane skin layers, the solution is forced
120 to move tangentially to the charged surfaces, pulling the excess of mobile ions within the electrical
121 double layers towards the low-pressure side. It results in an electrical current, known as the
122 streaming current (I_s), flowing between the membrane surfaces.

123 The standard theory implicitly assumes that the channel through which tangential streaming current
124 is measured has impermeable walls. If this condition is fulfilled and the distance between the surfaces
125 of the two membrane samples (h_{ch}) is much larger than the Debye length of the measuring solution,
126 the zeta potential (ζ) can be inferred from the streaming current by means of the well-known
127 Smoluchowski equation:

$$128 \quad I_s = - \frac{Wh_{ch}\varepsilon_0\varepsilon_r\Delta P}{\eta L} \zeta \quad (1)$$

129 where W and L are the channel width and length, respectively, ε_0 the vacuum permittivity (8.854×10^{-12}
130 F m^{-1}), ε_r and η the dielectric constant and the dynamic viscosity of the electrolyte solution,
131 respectively, and ΔP is the pressure difference applied between the channel ends.

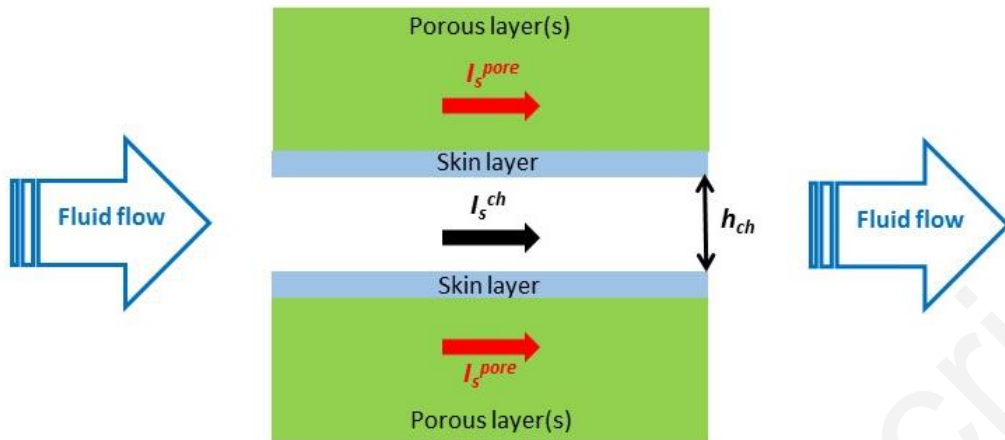
132 Although Eq. (1) is reliable for dense materials, it may break down when applied to ion-permeable
 133 materials such as micro- and ultra-filtration membranes, especially if the electrokinetic cell has been
 134 designed in such a way that it leaves the membrane support layer(s) exposed to the hydrodynamic
 135 flow during streaming current measurements [26, 28]. The reason is that a non-negligible streaming
 136 current is likely to flow through the membrane porous structure, which is filled with the measuring
 137 solution. This additional streaming current that we shall refer to as “electrokinetic leakage” is not
 138 accounted for in Eq. (1), which implicitly assumes that the experimental streaming current only flows
 139 along the membrane surfaces. For a given membrane, the occurrence of electrokinetic leakage can be
 140 easily confirmed or invalidated by measuring the streaming current for (at least) two different values
 141 of h_{ch} . Indeed, in the case of electrokinetic leakage, the (apparent) zeta potential that would be
 142 obtained by means of Eq. (1) would become dependent upon the distance between the membrane
 143 samples.

144 Eq. (2) has been proposed by Yaroshchuk and Luxbacher [26] to account for the contribution of
 145 electrokinetic leakage (see schematic description given in Fig. 1):

$$146 \quad I_s^{tot} = I_s^{ch} + 2I_s^{pore} = - \left(\frac{Wh_{ch}\epsilon_0\epsilon_r\Delta P}{\eta L} \zeta_{surf} + \frac{2Wh_{mb}^{eff}\epsilon_0\epsilon_r\Delta P}{\eta L} \zeta_{pore} \right) \quad (2)$$

147 Where I_s^{tot} , I_s^{ch} and I_s^{pore} are the total streaming current (i.e. the current measured experimentally),
 148 the streaming current flowing through the channel (i.e. between the membrane surfaces) and the
 149 electrokinetic leakage occurring within a single membrane, respectively, ζ_{surf} and ζ_{pore} are the zeta
 150 potentials of the membrane surface and inside the membrane porous body, respectively, and h_{mb}^{eff} the
 151 effective height where the electrokinetic leakage takes place in a single membrane (it includes the
 152 membrane thickness, porosity and tortuosity).

153



154
 155 **Figure 1: Schematic representation of the streaming current distribution when tangential**
 156 **electrokinetic measurements are carried out with porous membranes. The streaming current does not**
 157 **flow only between the membrane surfaces but also through the membranes porous body. The**
 158 **experimental streaming current is then equal to $I_s^{ch} + 2I_s^{pore}$.**

159
 160 It is worth mentioning that, unlike Eqs. (1) and (2), the softwares associated with the current
 161 commercial electrokinetic analyzers use an arbitrary convention stating that the measured streaming
 162 current and the zeta potential(s) are of the same sign. This convention will be used in the rest of this
 163 manuscript.

164 According to Eq. (2), the correct value of the zeta potential of the membrane surface can be
 165 determined by carrying out a series of streaming current measurements with various channel heights
 166 (h_{ch}). Indeed, ζ_{surf} can be obtained from the slope of I_s^{tot} vs. h_{ch} while the total electrokinetic leakage
 167 ($2I_s^{pore}$) is given by the y-intercept (the streaming current that would be measured if the two
 168 membrane surfaces were brought into contact, i.e. $h_{ch} = 0$). Eq. (2) also shows that the zeta potential
 169 inside the membrane porosity can be determined from the electrokinetic leakage provided if h_{mb}^{eff} is
 170 known, which can be achieved by means of additional electric conductance measurements for various
 171 h_{ch} . Indeed, considering the system described in Fig. 1 the following expression for the cell
 172 conductance (G_{cell}) can be derived [26,28]:

173
$$G_{cell} = \frac{W}{L} (h_{ch} \lambda_0 + 2h_{mb}^{eff} \lambda_{mb}) \quad (3)$$

174 Where λ_0 and λ_{mb} are the electric conductivities of the measuring solution in the channel between the
175 membrane surfaces and inside the membrane pores, respectively.

176

177 **3 Materials and methods**

178 **3.1 Membranes**

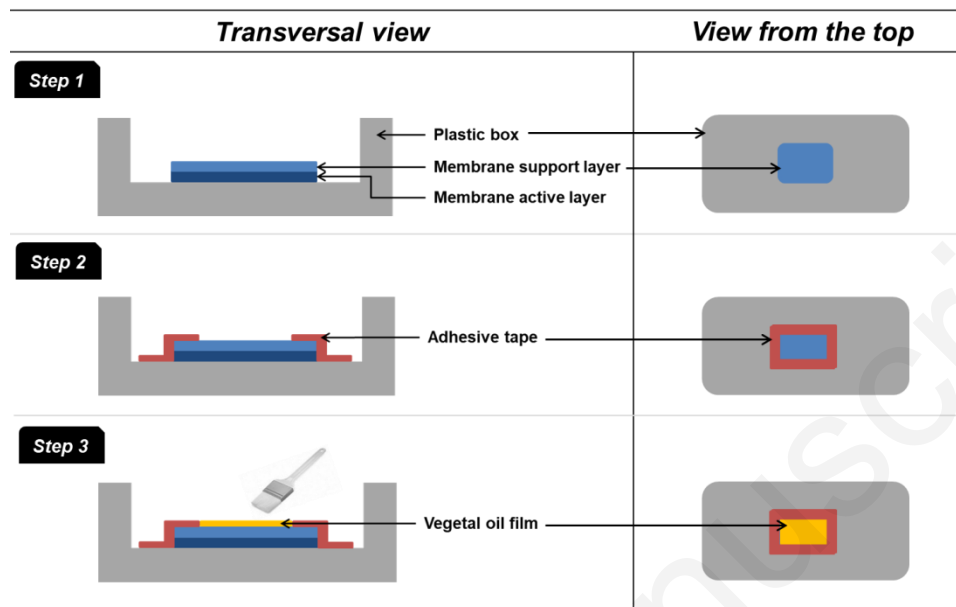
179 Two commercial flat-sheet membranes were used in this work: a microfiltration (MF)
180 polyethersulfone (PES) membrane with an average pore diameter of 0.1 μm (Koch, USA) and an
181 ultrafiltration (UF) polyacrylonitrile (PAN) membrane with a molecular weight cut-off (MWCO) of
182 500kDa (Orelis, France). The following protocol was followed to remove membrane preservatives
183 prior use: sonication first in a 50 v/v % water-ethanol mixture for 10 min followed by sonication in
184 deionized water (DI) water for 10 min (this last step was repeated twice).

185

186 **3.2 Membrane fouling**

187 **3.2.1 Lab-scale fouling experiments**

188 “Upside down” fouling experiments were performed in order to provide the proof of concept of the
189 methodology we propose in this work, which is based on the variation of the electrokinetic leakage
190 occurring in the porous structures of membranes as a result of internal fouling. The protocol is
191 schematically described in Fig. 2. The membrane coupons were fixed at the bottom of a plastic box
192 using adhesive tape, the membrane skin layer facing the bottom of the box (steps 1 and 2 in Fig. 2).
193 Then, commercial sunflower oil was poured onto the surface of the membrane support and
194 homogeneously spread with a paintbrush. Oil was then let diffuse through the membrane (from the
195 support towards the skin layer) for 4 hours at room temperature (step 3). The remaining oil on the
196 support surface was wiped with a tissue paper prior to membrane characterization.



198

199 **Figure 2: Experimental protocol for upside down fouling of membrane samples by vegetable oil.**

200

201 3.2.2 Pilot-scale fouling experiments

202 Pilot-scale fouling experiments were performed using a cross-flow filtration module (Rayflow X100,
 203 Orelis-Novasep, France) with a filtration area close to 130 cm². The feed cross-flow circulation was
 204 ensured by a peristaltic pump (ref 520S IP31, Watson-Marlow, USA), the cross-flow velocity being
 205 around 0.4 m.s⁻¹. Permeation through the membrane was ensured by applying a constant
 206 transmembrane pressure difference (TMP) adjusted with a back-pressure valve. Two pressure
 207 sensors placed at the module inlet and outlet on the retentate side allowed TMP monitoring and
 208 adjustment [29]. Before measurements, the membranes were first cleaned by successive filtrations
 209 of alkali solutions according to the following order: mixture of 0.1 g.L⁻¹ NaOH and 0.02 g.L⁻¹ NaClO
 210 solution at 30°C (pH ~ 10-11), followed by 2 g.L⁻¹ commercial Ultrasil 110 solution (Ecolab, France)
 211 at 45°C. Between each cleaning step, membranes were carefully rinsed in order to remove the
 212 remaining chemicals. To this end, successive filtrations of DI water (30°C) without permeate and
 213 retentate recirculation and under constant pressure of 0.2 bar were performed until the permeate
 214 reached the pH of DI water. At the end of the cleaning step, membranes were compacted by DI water

215 filtration at constant TMP (2 bar) and constant temperature ($30\pm 1^\circ\text{C}$) until a steady state water flux
216 was reached ($\pm 5\%$). The evolution of the permeate flux during the filtration process was measured
217 by collecting the permeate in a beaker placed on an electronic scale (model XL1200C, Precisa,
218 Switzerland).

219 After membrane compaction, DI water filtration pressure-stepping experiments (5 pressure steps
220 from 0.2 to 1.0 bar) were carried out in order to determine the 30°C water permeability of each
221 coupon.

222 Fouling experiments were further conducted using a 2% oil-in-water emulsion as the foulant feed (~
223 2 liters). It was used by some of us in a previous study as a model system representative of the
224 supernatant of a concentrated pretreated culture of *Parachlorella kessleri* microalgae, after bead
225 milling and separation of the cell fragments by centrifugation [29,30]. The aqueous phase had a pH of
226 7.4 and a conductivity of $790\ \mu\text{S cm}^{-1}$ and the lipid phase consisted in a mixture of vegetable oils
227 containing 70 wt% of neutral lipids and 30 wt% of polar lipids [29]. Fouling experiments were carried
228 out at two TMP (0.2 and 1.0 bar) so as to get different levels of fouling. Experiments were stopped
229 when a volume reduction ratio of 2 was achieved and the membranes were further rinsed by two
230 successive DI water filtrations under a TMP of 0.2 bar for 15 minutes in order to remove the reversible
231 part of fouling.

232

233 **3.3 Membrane characterization: Tangential streaming current**

234 Electrokinetic measurements were performed with a Surpass electrokinetic analyzer (Anton Paar
235 GmbH) equipped with an adjustable-gap cell requiring two membrane samples (each one $2 \times 1\ \text{cm}$)
236 [28]. For all experiments, the membranes were positioned in the adjustable-gap cell with their skin
237 layers facing each other (as shown schematically in Fig. 1). Experiments were performed at $T=22\pm 2$
238 $^\circ\text{C}$ with 500 mL of a 0.001 M KCl solution, the pH of which was adjusted in the range 4.50 – 5.00 with
239 a 0.05 M HCl solution and kept constant within ± 0.05 throughout the course of the experiment. Prior
240 to measurements, the solution was circulated through the channel for *ca.* 2 h to allow the sample
241 equilibration. After equilibration, the streaming current was measured and recorded for increasing
242 pressure differences (ΔP) up to 300 mbar. Measurements were repeated by progressively decreasing

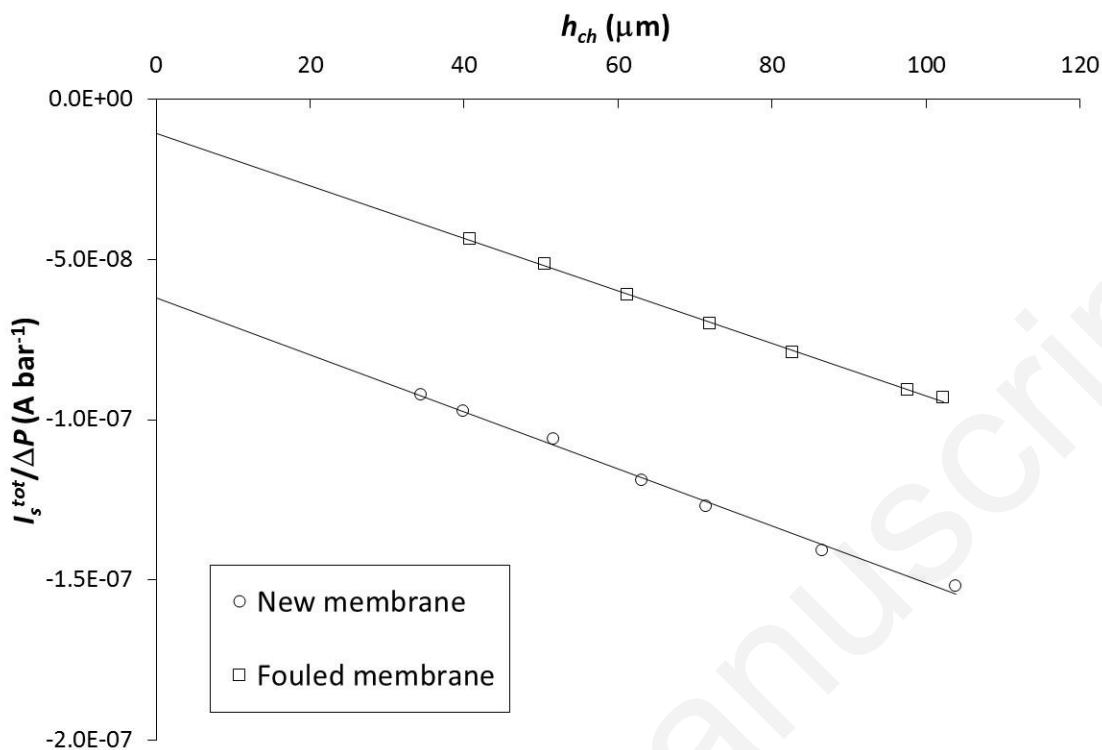
243 the distance between the membrane samples (h_{ch}) from $\sim 100 \mu\text{m}$ to $\sim 40 \mu\text{m}$ by means of the
244 micrometric screws of the adjustable-gap cell.

245 For some experiments, the electrical conductance of the adjustable-gap cell was also measured (for
246 various values of h_{ch}) in order to evaluate the effective height where the electrokinetic leakage takes
247 place in the membrane (h_{mb}^{eff}). For these additional measurements, a more concentrated KCl solution
248 (0.1 M) was used in order to minimize the impact of the electrical double layers on the electrical
249 conductivity inside the membrane pores [28].

250 **4 Results**

251 **4.1 Proof of concept**

252 In a preliminary work, the UF PAN membrane was first fouled according to the “upside down” fouling
253 protocol described in section 3.2.1 and schematically shown in Fig. 2. Next, two membrane samples
254 were positioned in the adjustable-gap cell of the electrokinetic analyzer with their skin layers facing
255 each other (as shown schematically in Fig. 1). For all experiments, a linear variation was observed
256 between the applied pressure and the resulting streaming current, making it possible to
257 unambiguously define the streaming current coefficient as the slope of the I_s^{tot} vs ΔP plots. Fig. 3 shows
258 the variation of the streaming current coefficient as function of the distance between the membrane
259 samples in the adjustable-gap cell (h_{ch}). As expected from Eq. (2), a linear variation was observed for
260 both new and fouled membrane samples.



261

262 **Figure 3: Streaming current coefficient of the pristine and fouled PAN membranes as function of the**
 263 **distance between the samples; measuring solution: 0.001 M KCl solution at pH 4.50 ±0.05.**

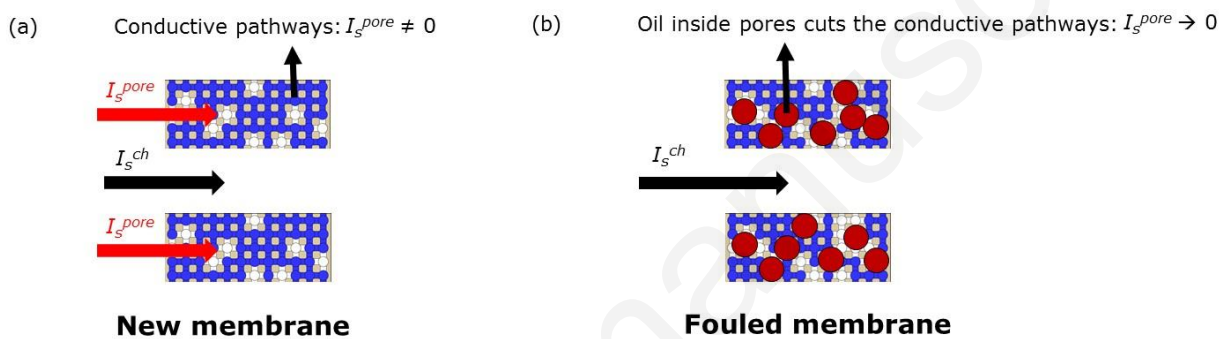
264

265 Extrapolating the streaming current coefficient of the pristine membrane down to $h_{ch} = 0$ (i.e.
 266 membrane surfaces in contact with no longer a channel in between) gives evidence of the
 267 electrokinetic leakage phenomenon since the y-intercept differs from zero, as shown by Eq. (2). It was
 268 found to be $-6.2 \times 10^{-8} \text{ A} \cdot \text{bar}^{-1}$, which represents 40% of the experimental signal ($I_s^{tot}/\Delta P$) measured by
 269 setting the distance between the samples at $100 \mu\text{m}$ and up to 65% of the experimental signal if h_{ch} is
 270 set at $40 \mu\text{m}$. In the Supplementary Information of this manuscript, the reader can find additional
 271 measurements obtained with a track-etched membrane (Fig. S1). As expected, no electrokinetic
 272 leakage occurred since track-etched membranes have non-interconnected pores, thus preventing any
 273 tangential flow through the porous structure.

274 Interestingly, an almost six-fold decrease in the magnitude of the electrokinetic leakage was obtained
 275 after letting the support layer of the PAN membrane in contact with sunflower oil for four hours as
 276 described in section 3.2.1. These results can be explained as follows. With the pristine membranes,

277 the electrokinetic leakage phenomenon can take place because the membrane pores are filled with
 278 the electrolyte solution required for electrokinetic measurements, which creates ion-conductive
 279 pathways through which a part of the streaming current, $2I_s^{pore}$ in Eq. (2), can flow (see Fig. 4a); the
 280 magnitude of the electrokinetic leakage would increase with the membrane thickness, porosity,
 281 hydrophilicity and pore surface charge. Because of the hydrophobic character of oil, these conductive
 282 pathways are progressively clogged as oil penetrates into the membrane pores (Fig. 4b), which results
 283 in a weaker electrokinetic leakage as reported in Fig. 3.

284



285

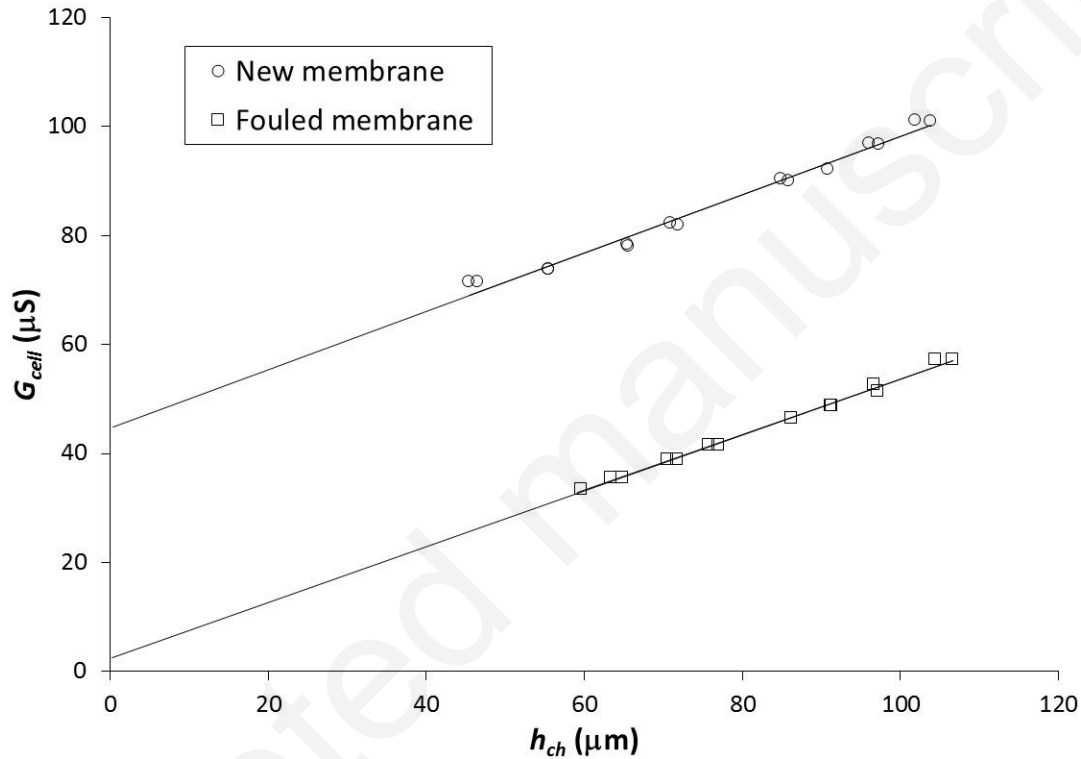
286 **Figure 4: Schematic representation of (a) open conductive pathways allowing electrokinetic leakage**
 287 **through the membrane porosity and (b) clogged conductive pathways leading to electrokinetic**
 288 **leakage disappearance.**

289 It is worth noting in Fig. 3 that the same slope was obtained in the electrokinetic response of both
 290 PAN membrane coupons. According to Eq. (2), this results means that the zeta potential of the skin
 291 layer surface (ζ_{surf}) was not impacted after membrane fouling. Otherwise stated, it means that oil
 292 entered the membrane pores from the support layer side but did not cross the membrane skin layer.

293 These results show that the proposed methodology makes it possible to separate the contribution of
 294 surface and internal fouling.

295 As stated in section 2, the effective height where the electrokinetic leakage takes place in a single
 296 membrane (h_{mb}^{eff}) can be estimated by means of additional electric conductance measurements. Fig.
 297 5 shows the variation of the cell conductance (G_{cell}) as function of h_{ch} . As predicted by Eq. (3), a linear
 298 variation of G_{cell} with h_{ch} was obtained for both new and fouled PAN membranes. A concentrated

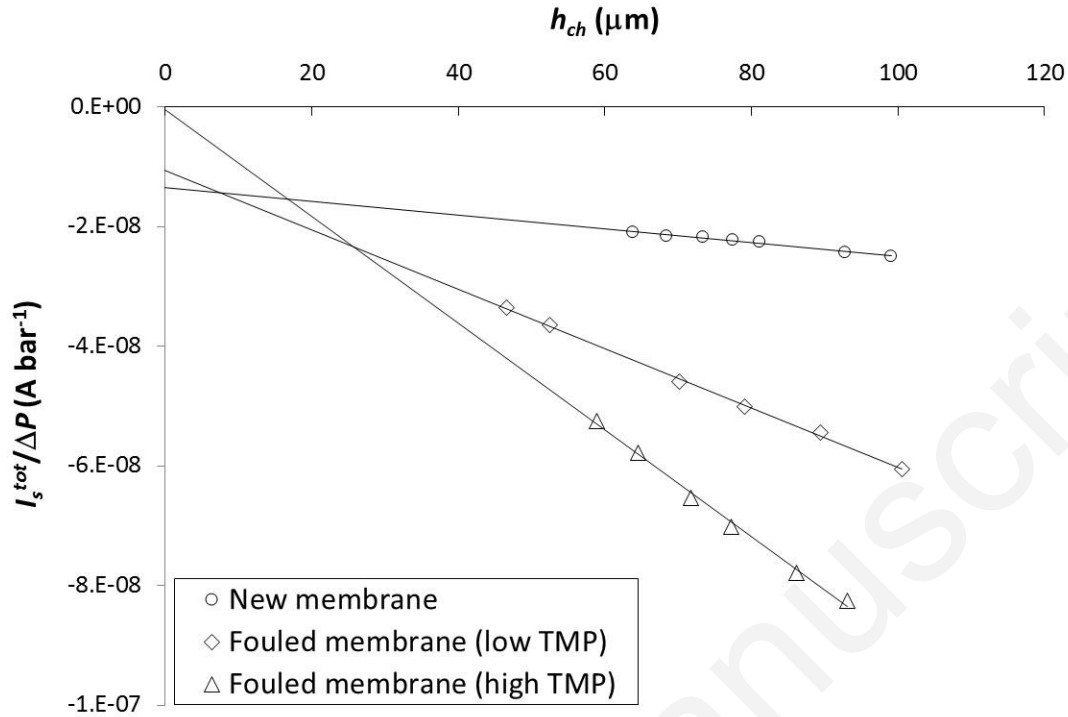
299 solution (0.1 M KCl) was used to minimize the impact of the electrical double layers on the electrical
 300 conductivity inside the membrane pores and to reasonably assume $\lambda_{mb} \approx \lambda_0$ [28]. The h_{mb}^{eff} values for
 301 both membranes were inferred from the y-intercept according to Eq. (3). For the pristine membrane,
 302 h_{mb}^{eff} was found to be about 40 μm while it fell down to 2 μm for the fouled membrane, thus confirming
 303 that the presence of oil inside the membrane pores cut the conduction pathways responsible for the
 304 electrokinetic leakage phenomenon.



305
 306 **Figure 5: Cell conductance measured with the PAN membranes as a function of the distance between**
 307 **the samples; measuring solution: 0.1 M KCl solution at pH 4.50 \pm 0.05.**

308
 309 **4.2 Application to oil-in-water emulsion filtration**

310 Pilot-scale filtration experiments were then conducted on the 2% oil-in-water emulsion using MF PES
 311 and UF PAN membranes. Fig. 6 shows the variation of the streaming current coefficient of the MF PES
 312 membrane as function of the distance between the membrane samples in the adjustable-gap cell (h_{ch}).



313

314 **Figure 6: Streaming current coefficient of the pristine and fouled PES membranes as function of the**
 315 **distance between the samples; measuring solution: 0.001 M KCl solution at pH 5.00 ±0.05.**

316

317 Different electrokinetic responses were obtained for the pristine membrane and the membranes
 318 fouled by filtering the 2% oil-in-water emulsion described in section 3.2.2.

319 The slope of the electrokinetic response was found to increase with fouling, being even steeper after
 320 filtration at high TMP (1 bar). Since the slope of the $I_s^{tot}/\Delta P$ vs h_{ch} plot is proportional to ζ_{surf} (see Eq.
 321 (2)), it means that (i) the zeta potential of the foulant was higher than that of the bare membrane
 322 surface and (ii) the coverage of the PES membrane surface by the oil droplets (surface fouling)
 323 increased by applying a higher TMP. The values of ζ_{surf} can be straightforwardly deduced from Eq.
 324 (2) and are collected in Table 1.

325 A slight decrease in the electrokinetic leakage is observed after filtration of the emulsion at low TMP
 326 (0.2 bar). On the other hand, the electrokinetic leakage almost vanished after filtration at 1 bar (it was
 327 divided by a factor of 34 compared with the pristine membrane). These results indicate that a higher

328 TMP favored the penetration of the oil droplets into the porous structure of the 0.1 μm PES
329 membrane.

330 **Table 1: Surface zeta potentials (ζ_{surf}) of the various membranes inferred from Eq. (2).**

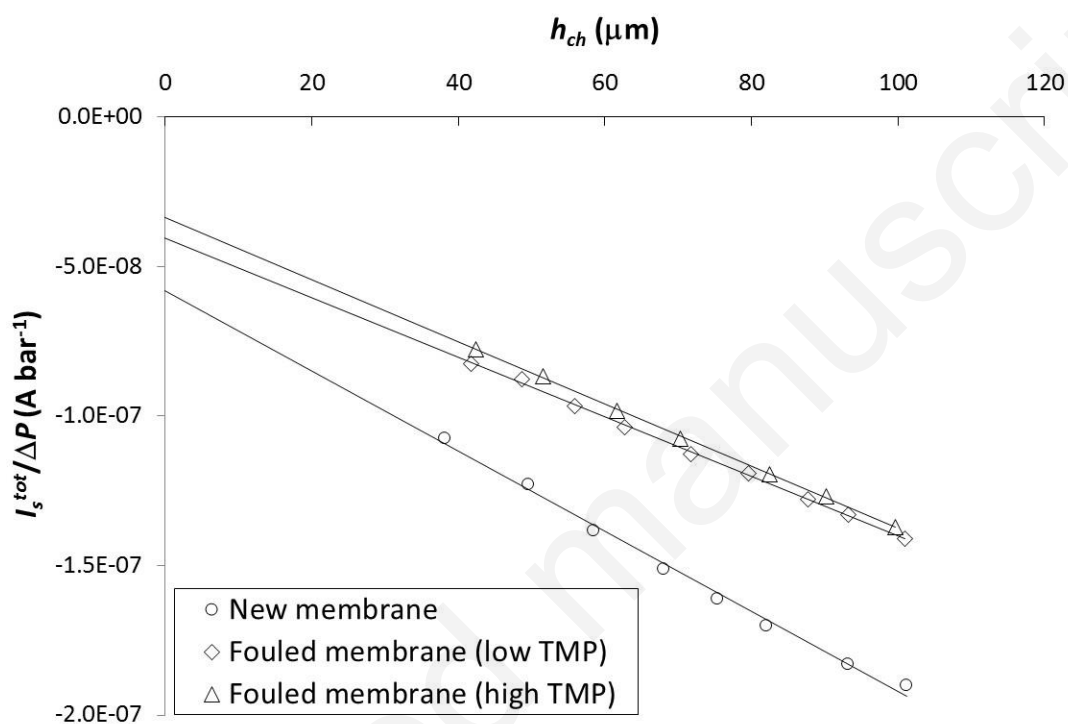
Membrane	Membrane surface zeta potential (mV)		
	New	Fouled (low TMP)	Fouled (high TMP)
PES 0.1 μm	-2.9 ± 0.9	-13.0 ± 0.6	-23.1 ± 1.4
PAN 500 kDa	-35.1 ± 1.0	-26.1 ± 2.9	-26.8 ± 2.3

331
332 It can be noted that the standard Smoluchowski equation (Eq. (1)) could be used with confidence to
333 compute the surface zeta potential of the PES membrane fouled at high TMP since the electrokinetic
334 leakage phenomenon was suppressed under these operating conditions: the surface zeta potential
335 determined from Eq. (1) with $h_{ch} = 100 \mu\text{m}$ and from Eq. (2) are -23.2 mV and -23.1 mV , respectively.
336 However it would overestimate the surface zeta potential of the new PES membrane and the
337 membrane fouled at low TMP by 117 % and 21 %, respectively (still considering data for $h_{ch} = 100$
338 μm in Eq. (1)).

339 A different behavior was observed with the 500 kDa UF PAN membrane. Indeed, as shown in Fig. 7,
340 the impact of the TMP on both the external and internal fouling was marginal since the electrokinetic
341 response (slope and y-intercept) of membranes fouled at low and high TMP were found to be very
342 close.

343 The surface of the PAN membrane was found to be more negatively charged than the PES membrane
344 (see Table 1). The slope of the electrokinetic response (and thus the surface zeta potential) was found
345 to slightly decrease after fouling, unlike what was observed with the PES membrane for which a strong
346 increase was reported (Fig. 6). It means that the foulant species from the emulsion were less
347 negatively charged than the pristine PAN membrane. The surface zeta potentials of both the new and
348 fouled PAN membranes are given in Table 1.

349 The PAN membrane appeared to be less prone to internal fouling by the oil-in-water emulsion than
 350 the PES membrane since the electrokinetic leakage occurring in the PAN and PES membranes
 351 decreased by a factor of 1.7 and 34, respectively, after fouling at high TMP. It results from to the more
 352 open porous structure of the MF PES membrane compared with the UF PAN membrane along with
 353 the more hydrophobic character of PES [10, 11] favoring interactions with the oil droplets.



354
 355 **Figure 7: Streaming current coefficient of the pristine and fouled PAN membranes as function of the**
 356 **distance between the samples; measuring solution: 0.001 M KCl solution at pH 5.00 ±0.05.**

357
 358 Interestingly, ζ_{surf} for the fouled PAN membranes and the PES membrane fouled at high TMP were
 359 found to be very close: -26.1, -26.8 and -23.1 mV for the PAN membrane fouled at low TMP, the PAN
 360 membrane fouled at high TMP and the PES membrane fouled at high TMP, respectively. Since the bare
 361 PAN and PES membranes had substantially different ζ_{surf} (-35.1 and -2.9 mV, respectively), this
 362 finding suggests that (i) the surface of both membranes was fully covered by foulant species from the
 363 emulsion and (ii) these foulant species develop an electrokinetic charge density in the

364 physicochemical environment considered in this study (0.001 M KCl at pH 5), which is characterized
365 by a zeta potential in the range from ~ -20 mV to ~ -30 mV.

366 Additional electrophoretic light scattering measurements were performed with the emulsion diluted
367 1000 times in a 0.001 M KCl solution at pH 5. The zeta potential of the emulsion droplets was found
368 to be -25.7 ± 1.1 mV, which confirms that the PES membrane surface was fully covered after filtration
369 at high TMP while that of the PAN membrane was covered even at low TMP.

370

371 **5 Conclusion**

372 The electrokinetic leakage, which is the part of the streaming current that flows through the porosity
373 of a membrane when tangential electrokinetic measurements are carried out, is a parasitic
374 phenomenon that makes more tedious the accurate determination of the surface zeta potential.
375 Nonetheless, since this parasitic contribution is sensitive to local changes inside the membrane
376 porosity it is likely to provide useful information when investigating problems of practical relevance.
377 In this study, we showed for the first time that electrokinetic leakage can serve as a probe for
378 detecting internal fouling in MF and UF membranes, taking lipidic fouling as example. Notably, it was
379 used to highlight the substantial impact of the TMP on the internal fouling of a MF PES membrane
380 caused by filtration of an oil-in-water emulsion. On the other hand, almost no impact of the TMP was
381 noticed in the case of a UF PAN membrane with narrower pores. Moreover, the experimental protocol
382 implemented here to quantify the electrokinetic leakage phenomenon allowed to distinguish between
383 the contribution of internal fouling and that of external (surface) fouling.

384 This paper offers new prospects for tangential electrokinetic measurements by providing an
385 innovative methodology for the characterization of internal fouling. These findings could find useful
386 application in MF and UF processes for which internal fouling is often responsible of severe
387 productivity decrease and laborious cleaning procedures. Moreover, in view of the vast volumes of
388 oily wastewater produced in various industrial fields (microalgae, food and beverages, oil and gas,
389 metal processing, etc.), the characterization of membrane fouling during oil-in-water emulsions
390 treatment is a key challenge for the development of cost-effective and eco-friendly processing
391 involving membranes filtration.

392 Interestingly, the methodology proposed in this work is not restricted to membrane fouling studies
393 and it could be applied straightforwardly to other topics of membrane science including membrane
394 functionalization and membrane degradation (physical or chemical ageing). A limitation of this
395 method is that it requires varying the spacing between the membranes, which makes it difficult to
396 apply it on-line with existing membrane modules.

397 **6 Acknowledgements**

398 Cédric Brossard (Malvern Panalytical) is gratefully acknowledged for electrophoretic light scattering
399 measurements. This work was supported by GIS Europôle Mer, France (Sciences et Ingénieries
400 Marines, 2016-2017), Université de Bretagne Loire, ADEME and the Challenge Food For
401 Tomorrow/Cap Aliment, Pays de la Loire, France.

402 **7 Bibliography**

- 403 [1] G. Rudolph, T. Virtanen, M. Ferrando, C. Güell, F. Lipnizki, M. Kallioinen, A review of in situ real-
404 time monitoring techniques for membrane fouling in the biotechnology, biorefinery and food
405 sectors, *J. Membr. Sci.* 588 (2019) 117221. doi:10.1016/j.memsci.2019.117221.
- 406 [2] D.J. Johnson, D.L. Oatley-Radcliffe, N. Hilal, State of the art review on membrane surface
407 characterisation: Visualisation, verification and quantification of membrane properties, *Rev.*
408 *Res. Dev. Desalination.* 434 (2018) 12–36. doi:10.1016/j.desal.2017.03.023.
- 409 [3] D. Delaunay, M. Rabiller-Baudry, J.M. Gozálvarez-Zafrilla, B. Balannec, M. Frappart, L. Paugam,
410 Mapping of protein fouling by FTIR-ATR as experimental tool to study membrane fouling and
411 fluid velocity profile in various geometries and validation by CFD simulation, *Euromembrane*
412 2006. 47 (2008) 1106–1117. doi:10.1016/j.cep.2007.12.008.
- 413 [4] M. Rabiller-Baudry, L. Bégoïn, D. Delaunay, L. Paugam, B. Chaufer, A dual approach of membrane
414 cleaning based on physico-chemistry and hydrodynamics: Application to PES membrane of
415 dairy industry, *10th Fr. Congr. Chem. Eng.* 47 (2008) 267–275. doi:10.1016/j.cep.2007.01.026.
- 416 [5] M.J. Luján-Facundo, J.A. Mendoza-Roca, B. Cuartas-Urbe, S. Álvarez-Blanco, Evaluation of
417 cleaning efficiency of ultrafiltration membranes fouled by BSA using FTIR-ATR as a tool, *J. Food*
418 *Eng.* 163 (2015) 1–8. doi:10.1016/j.jfoodeng.2015.04.015.
- 419 [6] A. Yeo, P. Yang, A.G. Fane, T. White, H.O. Moser, Non-invasive observation of external and internal
420 deposition during membrane filtration by X-ray microimaging (XMI), *J. Membr. Sci.* 250 (2005)
421 189–193. doi:10.1016/j.memsci.2004.10.035.

- 422 [7] T.A. Trinh, W. Li, Q. Han, X. Liu, A.G. Fane, J.W. Chew, Analyzing external and internal membrane
423 fouling by oil emulsions via 3D optical coherence tomography, *J. Membr. Sci.* 548 (2018) 632–
424 640. doi:10.1016/j.memsci.2017.10.043.
- 425 [8] M.C. Martí-Calatayud, S. Schneider, M. Wessling, On the rejection and reversibility of fouling in
426 ultrafiltration as assessed by hydraulic impedance spectroscopy, *J. Membr. Sci.* 564 (2018) 532–
427 542. doi:10.1016/j.memsci.2018.07.021.
- 428 [9] J. Benavente, G. Jonsson, Effect of adsorbed protein on the hydraulic permeability, membrane
429 and streaming potential values measured across a microporous membrane, *Colloids Surf.*
430 *Physicochem. Eng. Asp.* 138 (1998) 255–264. doi:10.1016/S0927-7757(97)00119-2.
- 431 [10] L. Marbelia, M. Mulier, D. Vandamme, K. Muylaert, A. Szymczyk, I.F.J. Vankelecom,
432 Polyacrylonitrile membranes for microalgae filtration: Influence of porosity, surface charge and
433 microalgae species on membrane fouling, *Algal Res.* 19 (2016) 128–137.
434 doi:10.1016/j.algal.2016.08.004.
- 435 [11] Y. Hanafi, A. Szymczyk, M. Rabiller-Baudry, K. Baddari, Degradation of Poly(Ether
436 Sulfone)/Polyvinylpyrrolidone Membranes by Sodium Hypochlorite: Insight from Advanced
437 Electrokinetic Characterizations, *Environ. Sci. Technol.* 48 (2014) 13419–13426.
438 doi:10.1021/es5027882.
- 439 [12] Y. Hanafi, P. Loulergue, S. Ababou-Girard, C. Meriadec, M. Rabiller-Baudry, K. Baddari, A.
440 Szymczyk, Electrokinetic analysis of PES/PVP membranes aged by sodium hypochlorite
441 solutions at different pH, *J. Membr. Sci.* 501 (2016) 24–32. doi:10.1016/j.memsci.2015.11.041.
- 442 [13] M. Nyström, A. Pihlajamäki, N. Ehsani, Characterization of ultrafiltration membranes by
443 simultaneous streaming potential and flux measurements, *J. Membr. Sci.* 87 (1994) 245–256.
444 doi:10.1016/0376-7388(94)87031-4.
- 445 [14] I.H. Huisman, P. Prádanos, A. Hernández, Electrokinetic characterisation of ultrafiltration
446 membranes by streaming potential, electroviscous effect, and salt retention, *J. Membr. Sci.* 178
447 (2000) 55–64. doi:10.1016/S0376-7388(00)00479-8.
- 448 [15] M. Sbaï, P. Fievet, A. Szymczyk, B. Aoubiza, A. Vidonne, A. Foissy, Streaming potential,
449 electroviscous effect, pore conductivity and membrane potential for the determination of the
450 surface potential of a ceramic ultrafiltration membrane, *J. Membr. Sci.* 215 (2003) 1–9.
451 doi:10.1016/S0376-7388(02)00553-7.
- 452 [16] A. Szymczyk, C. Labbez, P. Fievet, B. Aoubiza, C. Simon, Streaming potential through multilayer
453 membranes, *AIChE J.* 47 (2001) 2349–2358. doi:10.1002/aic.690471019.
- 454 [17] A.E. Yaroshchuk, Y.P. Boiko, A.L. Makovetskiy, Filtration Potential across Membranes Containing
455 Selective Layers, *Langmuir.* 18 (2002) 5154–5162. doi:10.1021/la025503s.
- 456 [18] P. Fievet, M. Sbaï, A. Szymczyk, Analysis of the pressure-induced potential arising across
457 selective multilayer membranes, *J. Membr. Sci.* 264 (2005) 1–12.
458 doi:10.1016/j.memsci.2005.04.011.

- 459 [19] D. Möckel, E. Staude, M. Dal-Cin, K. Darcovich, M. Guiver, Tangential flow streaming potential
460 measurements: Hydrodynamic cell characterization and zeta potentials of carboxylated
461 polysulfone membranes, *J. Membr. Sci.* 145 (1998) 211–222. doi:10.1016/S0376-
462 7388(98)00077-5.
- 463 [20] P. Fievet, M. Sbaï, A. Szymczyk, C. Magnenet, C. Labbez, A. Vidonne, A New Tangential Streaming
464 Potential Setup for the Electrokinetic Characterization of Tubular Membranes, *Sep. Sci. Technol.*
465 39 (2004) 2931–2949. doi:10.1081/SS-200028652.
- 466 [21] V.T. Do, C.Y. Tang, M. Reinhard, J.O. Leckie, Degradation of Polyamide Nanofiltration and Reverse
467 Osmosis Membranes by Hypochlorite, *Environ. Sci. Technol.* 46 (2012) 852–859.
468 doi:10.1021/es203090y.
- 469 [22] S. Liu, C. Wu, X. Hou, J. She, S. Liu, X. Lu, H. Zhang, S. Gray, Understanding the chlorination
470 mechanism and the chlorine-induced separation performance evolution of polypiperazine-
471 amide nanofiltration membrane, *J. Membr. Sci.* 573 (2019) 36–45.
472 doi:10.1016/j.memsci.2018.11.071.
- 473 [23] A. Yaroshchuk, V. Ribitsch, Role of Channel Wall Conductance in the Determination of ζ -Potential
474 from Electrokinetic Measurements, *Langmuir.* 18 (2002) 2036–2038. doi:10.1021/la015557m.
- 475 [24] P. Fievet, M. Sbaï, A. Szymczyk, A. Vidonne, Determining the ζ -potential of plane membranes
476 from tangential streaming potential measurements: effect of the membrane body conductance,
477 *J. Membr. Sci.* 226 (2003) 227–236. doi:10.1016/j.memsci.2003.09.007.
- 478 [25] E. Idil Mouhoumed, A. Szymczyk, A. Schäfer, L. Paugam, Y.H. La, Physico-chemical
479 characterization of polyamide NF/RO membranes: Insight from streaming current
480 measurements, *J. Membr. Sci.* 461 (2014) 130–138. doi:10.1016/j.memsci.2014.03.025.
- 481 [26] A. Yaroshchuk, T. Luxbacher, Interpretation of Electrokinetic Measurements with Porous Films:
482 Role of Electric Conductance and Streaming Current within Porous Structure, *Langmuir.* 26
483 (2010) 10882–10889. doi:10.1021/la100777z.
- 484 [27] S. Déon, P. Fievet, C. Osman Doubad, Tangential streaming potential/current measurements for
485 the characterization of composite membranes, *J. Membr. Sci.* 423–424 (2012) 413–421.
486 doi:10.1016/j.memsci.2012.08.038.
- 487 [28] A. Szymczyk, Y.I. Dirir, M. Picot, I. Nicolas, F. Barrière, Advanced electrokinetic characterization
488 of composite porous membranes, *J. Membr. Sci.* 429 (2013) 44–51.
489 doi:10.1016/j.memsci.2012.11.076.
- 490 [29] L. Villafaña-López, E.C. Rivera, S. Liu, E. Couallier, M. Frappart, Shear-enhanced membrane
491 filtration of model and real microalgae extracts for lipids recovery in biorefinery context,
492 *Bioresour. Technol.* (2019) 121539. doi:10.1016/j.biortech.2019.121539.
- 493 [30] E. Clavijo Rivera, V. Montalescot, M. Viau, D. Drouin, P. Bourseau, M. Frappart, C. Monteux, E.
494 Couallier, Mechanical cell disruption of *Parachlorella kessleri* microalgae: Impact on lipid
495 fraction composition, *Bioresour. Technol.* 256 (2018) 77–85.
496 doi:10.1016/j.biortech.2018.01.148.

497
498
499
500
501
502
503
504
505
506
507
508
509
510
511
512
513
514
515
516

Accepted manuscript

517

518

Supplementary Information

519

520

Electrokinetic leakage as a tool to probe internal fouling in MF and UF membranes

522

523 C. Rouquié^{1,2,3}, S. Liu^{2,4}, M. Rabiller-Baudry¹, A. Riaublanc³, M. Frappart², E. Couallier^{2*}, A. Szymczyk^{1*}

524

525 ¹Univ Rennes, CNRS, ISCR (Institut des Sciences Chimiques de Rennes) – UMR 6226, F-35000 Rennes, France

526 ²CNRS, GEPEA, Université de Nantes, 37 Boulevard de l'université, BP 406, 44602 Saint-Nazaire cedex, France

527 ³INRA, BIA, Rue de la Géraudière, BP 71627, 44 316 Nantes Cedex 3, France

528 ⁴ADEME, 20 avenue du Grésillé, BP90406, 49004 Angers cedex 01, France

529

530 *Corresponding authors: anthony.szymczyk@univ-rennes1.fr, estelle.couallier@univ-nantes.fr

531

532 Number of pages: 2

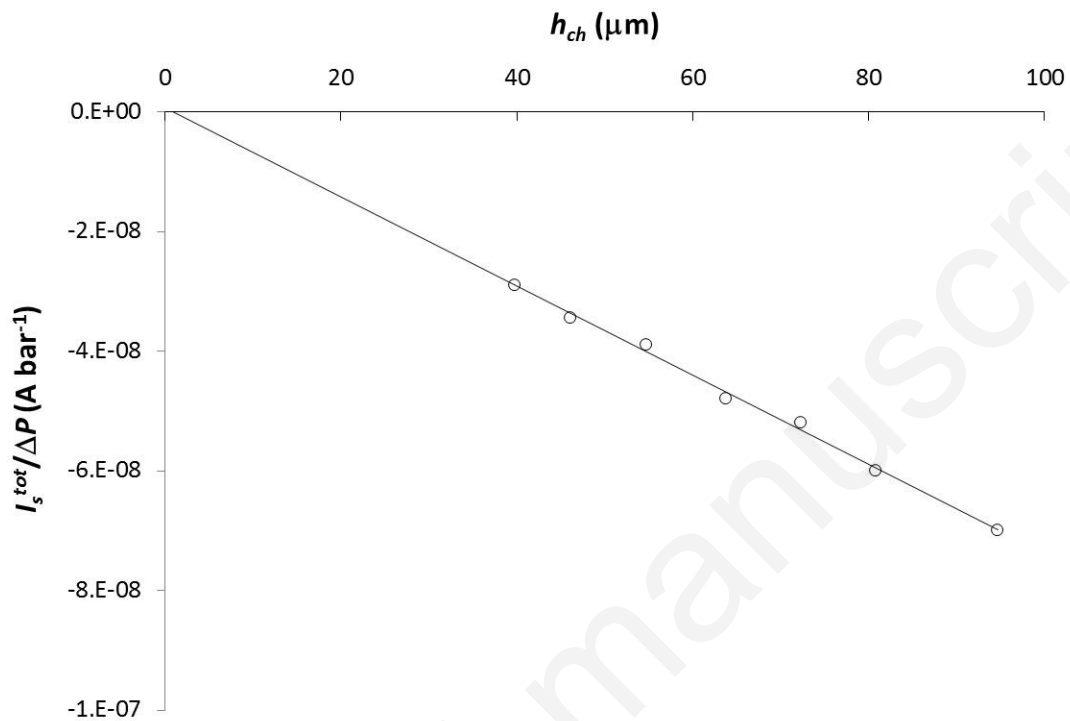
533 Number of Figures: 1

534

535

536

537



538

539 **Figure S1: Streaming current coefficient of a track-etched membrane as function of the distance**
540 **between the samples; measuring solution: 0.001 M KCl solution at pH 5.00 \pm 0.05.**

541

542

543

544

545

546